

# The End of an El Niño

## A VIEW FROM PALAU

By Martha C. Schönau, Hemantha W. Wijesekera, William J. Teague,  
Patrick L. Colin, Ganesh Gopalakrishnan, Daniel L. Rudnick, Bruce D. Cornuelle,  
Zachariah R. Hallock, and David W. Wang



R/V *Roger Revelle* approaches Malakal Harbor, Koror Island, Palau, in April 2017 during the Flow Encountering Abrupt Topography (FLEAT) program.

**ABSTRACT.** The ocean's response to the termination of the major 2015/2016 El Niño event was captured from moorings and gliders deployed near Palau as part of the Office of Naval Research Departmental Research Initiative Flow Encountering Abrupt Topography (FLEAT). As the El Niño transitioned to neutral conditions in spring 2016, pulses of positive (warm) sea surface height anomalies (SSHAs) moved westward, deepening the thermocline and reaching Palau by the end of March. Observations collected nearly two months after the arrival of the warm water revealed intraseasonal oscillations (ISOs) with periods of ~30 days and vertical displacements of isotherms exceeding ~100 m in the deeper part of the thermocline. Arrival of these warm anomalies coincided with the disappearance of the eastward flow associated with the North Equatorial Countercurrent, and anomalously large meridional velocities ( $0.4 \text{ m s}^{-1}$ ) and transports (~4–6 Sv) over the Kyushu-Palau Ridge on the northern edge of Palau. The 120-day, high-pass-filtered, satellite-acquired SSHAs showed packets of westward-moving waves with phase speeds of about  $0.2 \text{ m s}^{-1}$  at  $8.625^\circ\text{N}$ , with horizontal wavelengths and periods of about 550 km and 30 days, respectively. These waves, which appear to originate in the western Pacific, fall within the characteristics of mode-1 and mode-2 Rossby waves. Similar SSHAs were found near Palau following previous El Niño events, suggesting that formation of intraseasonal oscillations is part of an oceanic response to the termination of El Niño. The transition from El Niño to neutral conditions can affect the coral ecosystem around Palau by creating anomalous circulation and strong thermal anomalies extending from the surface to bottom waters deeper than 150 m, far below the depth limit of coral growth in Palau.

**IN PLAIN WORDS.** At Palau, an El Niño can reduce sea level and cool temperatures on the coral reefs. When the 2015/16 El Niño ended, a rapid increase in sea level was accompanied by strong northward circulation and return of warm water in a series of oscillations that changed temperatures along the reefs. The oscillations associated with this adjustment may have been helpful to the reef ecosystem by preventing potentially harmful, sustained high temperatures.

## INTRODUCTION

Palau is an island chain of 200 limestone and basaltic islands on the Kyushu-Palau Ridge located in the far western Pacific Ocean at a mean latitude of about  $7.5^\circ\text{N}$  (Figure 1). The topography, which ranges from mountains to low coral islands surrounded by large barrier reefs, changes rapidly from 10 m in depth at the outer edge to over 4,000 m depth at the ocean floor. The coral reefs that surround Palau are the cornerstone of its tourist economy. In 2018, 115,000 tourists visited Palau, five times greater than its population of 22,000. Tourism contributes to over half of Palau's gross domestic product (<https://www.palau.gov.pw/>). The coral reefs, ranging from shallow to deep mesophotic (low-light), attract an array of sea life, including hard and soft coral, 1,500 species of fish, giant clams,

jellyfish, and sharks (Colin, 2009). As Palau has aggressively moved to protect these areas for sustainable ecotourism, it also must contend with the large-scale ocean-atmosphere dynamics of the tropical Pacific.

North of Palau, the southern arm of the North Pacific Subtropical Gyre, the North Equatorial Current (NEC), flows westward (Figure 1a). South of Palau, the North Equatorial Countercurrent (NECC) returns subtropical and tropical waters eastward. Although Palau's area is small, its location between two large equatorial currents and its abrupt topography mean the island chain can influence and be impacted by multiscale regional ocean dynamics. There is considerable vertical structure to the currents in the region, with strong subthermocline flow running counter to that of the surface currents

(Qiu et al., 2013; Schönau and Rudnick, 2015). Recirculation around Palau is also common, with quasi-permanent eddies (Hacker et al., 1989; Kashino, 2013) and seasonal springtime recirculation of the NECC to the NEC as part of the Mindanao Dome (MD; Masumoto and Yamagata, 1991). At Palau, the NEC and NECC interact with the topography, creating strong internal tides that can cause large fluctuations in subsurface temperature on diurnal and semidiurnal time-scales (Wolanski, et al., 2004). Wind and currents contribute to the health of the reef ecosystem by enhancing upwelling and mixing, thus increasing the availability of nutrients (Wolanski et al., 2004; Colin, 2009). However, with this dynamic environment, the diverse ecosystem is at risk when large changes occur to the ambient circulation, which can happen interannually through variability of the El Niño-Southern Oscillation (ENSO), a major ocean-atmosphere coupled phenomenon that is rooted in the circulation and wind patterns of the tropical Pacific.

Each ENSO event is unique, and there is debate about the initialization, termination, and impacts of different events (Clarke, 2014; Santoso, 2019). Therefore, all observations of El Niño and associated events improve our understanding of both their predictability and impact. To give an example of ENSO dynamics, McPhaden (1999) provides a detailed description of the genesis and evolution of the 1997/98 El Niño, which is characteristic of many El Niño events. The 1997/98 El Niño was well monitored on the surface, owing to the establishment of the Tropical Atmosphere Ocean (TAO) array and advances in satellite observations. Prior to the event, there was an anomalous buildup of warm water in the far western Pacific. This buildup of heat may have contributed to westerly wind bursts from Madden-Julian Oscillations (MJOs), which then disrupted the trade winds over the equatorial Pacific. These western Pacific wind anomalies forced intraseasonal equa-

torial Kelvin waves that traveled eastward along the equator, depressing the thermocline and westward-propagating Rossby waves that shoaled the thermocline. The flattened thermocline allowed eastward movement of warm western-equatorial water, decreasing the zonal sea surface-temperature (SST) gradient along the equator and further weakening the trade winds. The movement of this warm water affects global weather patterns and ocean circulation, with a large impact on SST, sea level, and rainfall across the tropical Pacific (<https://earthobservatory.nasa.gov/features/ElNino>; Wyrтки, 1975; McPhaden, 1999, 2008; Vecchi and Harrison, 2000; Meyers et al., 2007). In mid-May 1998, a reappearance of equatorial trade winds forced equatorial upwelling, terminating the El Niño (McPhaden, 1999). The end of El Niño is thought to result from a combination of a discharge of equatorial waters from the equator, the reflection of planetary waves at the

oceanic boundaries, and stochastic wind processes (Wang and Picaut, 2004).

Various indices are used to define ENSO events, but typically both El Niño events and their opposites, La Niña events, are monitored by the zonal distribution of surface warm water along the equatorial Pacific. Their strengths are often compared using the average temperature over an area called the Niño 3.4 region (5°N–5°S, 120°W–170°W). The five-month running mean of the monthly temperature anomaly in this region is called the Niño 3.4 index, and the three-month average temperature anomaly in the region is called the Oceanic Niño Index (ONI) (<https://climatedataguide.ucar.edu/climate-data/nino-sst-indices-nino-12-3-34-4-oni-and-tni>). Simple diagrams depicting normal and El Niño conditions are shown in **Figure 2a and 2b**, respectively. Exceptionally large El Niño events occurred in 1982/83, 1997/98, and 2015/16.

Near Palau, ENSO variability has a

large impact. During El Niño, the currents around Palau—the NEC, NECC, and MC—have been reported to increase in magnitude (Hu et al., 2015), and the NECC meanders southward (Hsin and Qiu, 2012). Two decades of observations from vertical temperature logger arrays along Palau’s reefs (2000–present; Colin, 2009, 2018), and sustained glider operations near Palau (2009–2017; Schönau and Rudnick, 2015, 2017) have captured some of the strength of this interannual variability. El Niños are associated with periods of low sea level near Palau, with exposed reefs, low SST, and drought as the Walker cell moves eastward (**Figure 2b**). As the sea level decreases, the thermocline shoals, introducing cold water to the reef that can cause cold-water bleaching at the lower depth limits of coral growth (Colin, 2018). La Niña can be even more devastating, as deep thermoclines lead to anomalously warm water temperatures of 29°C to over 30°C at depths of 60 m to 90 m (Colin, 2018). These high temperatures can create a 90% rate of coral bleaching and die-off, such as during the 1998 La Niña (Bruno et al., 2001).

The FLEAT (Flow Encountering Abrupt Topography) project sponsored by the Office of Naval Research (ONR) enabled mooring and glider observations of the oceanic response at the end of 2015/16 El Niño near Palau. The response is evaluated using a regional numerical state estimate and satellite observations. The 2015/16 El Niño was comparable in strength and dynamics to the 1997/98 event (<https://www.cpc.ncep.noaa.gov/data/indices/sstoi.indices>; Jacox et al., 2016; L’Heureux et al., 2017; Santoso et al., 2017). The wind forcing that occurs at the end of an El Niño generates westward-propagating Rossby waves. These large shifts in energy and momentum can create high-frequency variability, unpredictable currents, and deepening of the thermocline near Palau. Observations from satellites and a numerical state estimate are used to track the basin-wide ocean adjustment in the tropical North Pacific during the tran-

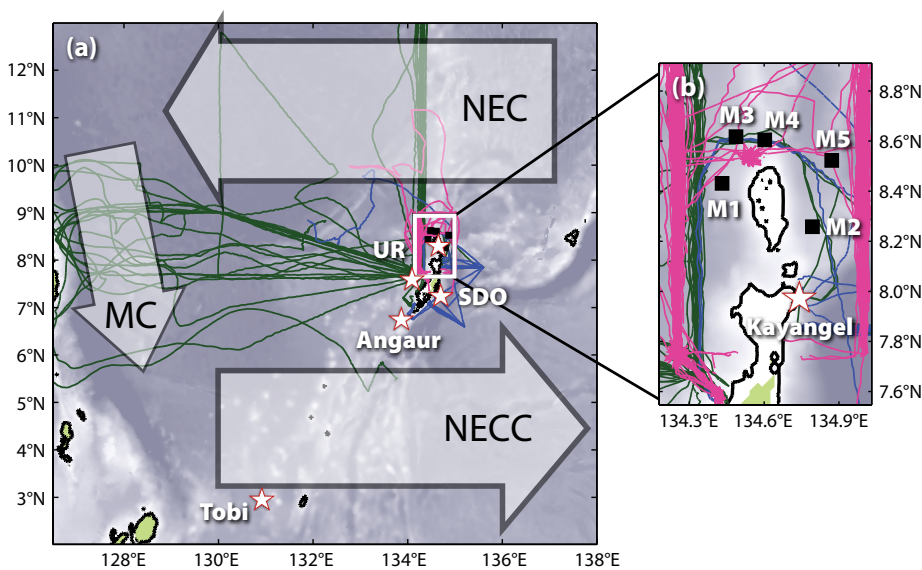


**FIGURE 1.** Overview of observations used to detail the end of the 2015/16 El Niño. (a) Bathymetry (shading), mooring, temperature logger, and glider observations around Palau. Glider observations were made from 2009 to 2014 (green) during the Origins of Kuroshio on Mindanao Current (OKMC) initiative, and during 2014 (blue) and 2015–2018 (pink) for the Flow Encountering Abrupt Topography (FLEAT) initiative. Arrows indicate large currents near Palau: the North Equatorial Current (NEC), the Mindanao Current (MC), and the North Equatorial Countercurrent (NECC). Not shown are the sub-thermocline currents and recirculations described in the text. (b) An expanded view of observations near the sunken atoll Velasco Reef (Ngeruangel). M1–M5 are deep subsurface acoustic Doppler current profiler (ADCP) moorings (2016–2017); four additional shallow, bottom-mounted ADCP moorings were also in place for FLEAT, but are not shown. Vertical temperature logger arrays, extending from the surface to 90 m depth are indicated at (a) Tobi (Hatohobei), Angaur, Ulong Rock (UR), Short Drop Off (SDO), and (b) Kayangel Atoll. The locations indicated here are components of a broader network of vertical temperature logger arrays deployed around Palau.

sition of the 2015/16 El Niño to normal conditions. FLEAT moorings and gliders, and vertical temperature logger arrays provide observations of how this transition occurred near Palau. From these observations, we infer how the temperature variability and timescales associated with the ENSO transition may impact the coral reef ecology.

The next section briefly describes the data collected. We then present a large-scale view of the termination of the ENSO event from satellite observations and a numerical state estimate, followed by the hydrographic and velocity fields from gliders, moorings, and thermographs. Our final sections discuss our findings, and a summary concludes the paper.

## METHODS: GLIDERS, MOORINGS, SATELLITES, AND A STATE ESTIMATE

To observe the El Niño and its subsequent decay in the western Pacific, we utilize observations from autonomous underwater gliders, vertical temperature logger arrays, and moorings near Palau, satellite observations, and solutions from a data-assimilating numerical ocean model. This combination of data and model solutions provides a description of the transition of currents near Palau, and a regional view of the dynamics and relevant forcing.

### Glider Observations

Spray gliders were first deployed from Palau during the ONR-sponsored Origins of the Kuroshio and Mindanao Current (OKMC) project (2009–2014; Rudnick et al., 2015; Schönau and Rudnick, 2015, 2017), and then for the FLEAT project (2015–2018; Zeiden et al., 2019; Figure 1a). The Spray gliders used during FLEAT were each equipped with a Sea-Bird CTD, chlorophyll fluorometers, and acoustic Doppler current profilers (ADCPs). The Spray glider is buoyancy controlled, descends to a depth of 1,000 m over a horizontal distance of 3 km, and collects data upon ascent over a similar horizontal distance. At the surface, the glider communicates via Iridium

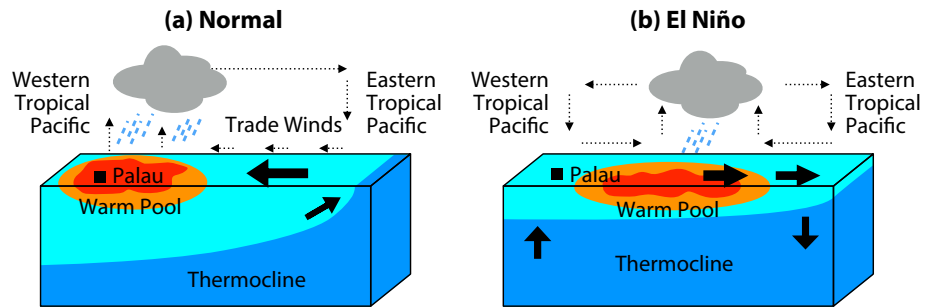


**FIGURE 2.** Schematic of the tropical Pacific during (a) normal and (b) El Niño conditions, based on diagrams in McPhaden et al. (1998). During normal conditions and La Niña conditions (not shown), trade winds maintain the warm pool in the western tropical Pacific, allowing for normal convection, a deeper thermocline, and normal to above average sea surface height (SSH). During an El Niño, westerly wind bursts can result in decreased trade winds and eastward movement of the warm pool, leading to a shoaling thermocline and decreased SSH in the western tropical Pacific.

satellite, telemetering data and receiving GPS coordinates. Further details of glider operations can be found in Rudnick et al. (2004).

During FLEAT, two gliders were typically deployed simultaneously, one on each side of Palau’s northern reef, to capture the interaction of the large-scale changes in the NEC as it flowed around the abrupt reef/island topography (Figure 1a). From 2015 to 2018, the 15 gliders deployed collected 7,000 profiles. Here, glider data taken near Palau during FLEAT are combined to estimate temperature and salinity near Palau. For this purpose, horizontal gradients are disregarded, as they are likely smaller than the vertical and temporal changes.

### Temperature Logger Stations

Vertical temperature logger arrays were instrumented at various stations along Palau’s reef in 2000, following the 1998 La Niña event that led to extreme coral bleaching (Colin, 2018). The arrays consist of Sea-Bird SBE56 temperature recorders and Onset HOBO U22-001 temperature data loggers, both pressure-protected thermistors. The arrays near the main Palau group have instruments ranging from 2 m to 90 m depth that sample at 30-minute intervals and are calibrated to 0.1°C. Here, we use data from four stations on either side of Palau: Kayangel Atoll, Ulong Rock (UR), Short Drop Off (SDO), and Angaur Island,

and from the station at Tobi (Hatohebei) Island, some 600 km southwest of the main Palau Group (Figure 1a). Tobi has a temperature logger at 57 m depth. These in situ temperature data are available from the Coral Reef Research Foundation’s Water Temperature Catalog (<http://wtc.coralreefpalau.org/>), and further details of instruments and calibration can be found in supplementary material from Schramek et al. (2018).

### Moorings

The FLEAT observational program consisted of year-long mooring deployments, from May 2016 to April 2017. A detailed discussion of instrumentation, data collection, sampling methods, and data processing of mooring observations during FLEAT is being prepared by authors Wijesekera, Teague, Wang, and Hallock; here, we describe a subset of the data that is relevant to this study. Five deep ADCP moorings were deployed around the sunken atoll of Velasco Reef (Ngeruangel; Figure 1b) in May 2016. Two of the moorings (M1 and M3) were deployed west of the reef in deep water (>2,600 m) and two moorings (M2 and M5) were deployed east of the reef at similar water depths (Figure 1b). M4 was deployed north of the reef plateau between M3 and M5 at 1,350 m depth. These deep moorings each contained an upward-looking ADCP operating at 300 kHz (Teledyne RD Instruments Workhorse) and a

downward-looking ADCP operating at 75 kHz (Teledyne RD Instruments Long Ranger), with both ADCPs mounted within a flotation ball at water depths between 64 m and 91 m (Figure 3). The moorings were designed to measure currents in the upper 600 m of the water column. The inertial period ranges from 80 hours to 84 hours at the mooring locations. Four additional moorings were deployed near the northern tip of Velasco

Reef in shallow water, but these data are not utilized here. Although the moorings were not in place until the 2015/16 El Niño had officially ended, the moorings provide time series of currents and northward transport in the vicinity of the reef following its termination. Table 1 provides positions, measurement depths, measurement times, sampling intervals, water depths, and instrument types.

was previously distributed by AVISO. The correlation coefficient between the monthly mean sea level anomaly in Malakal Harbor, Koror, Palau, and the corresponding SSHA from 1993 to 2016 was 0.99. Monthly averaged 10 m wind was obtained from the European Centre for Medium-Range Weather Forecasts (ECMWF) ERA-Interim reanalysis (Dee et al., 2011; <https://www.ecmwf.int>).

### Satellite Observations

Satellite products, consisting of SST, sea surface height anomalies (SSHAs), and 10 m winds are used to observe the basin-wide changes across the tropical Pacific Ocean during the end of the 2015/16 El Niño. SST is obtained from the monthly GLORYS12V1 reanalysis product (1993–present), gridded at 0.083° horizontal resolution, available from Copernicus Marine Environment Monitoring Service (CMEMS; <http://marine.copernicus.eu>). SSHAs and the associated geostrophic velocities are from the daily global ocean gridded L4 sea surface heights and derived variables (reprocessed, 1993–present), gridded at 0.25°, although the typical temporal resolution is close to seven days. The SSHA product is available from CMEMS, but

### Western Pacific Ocean

#### State Estimate

The Western Pacific Ocean State Estimate (WPOSE, <http://www.ecco.ucsd.edu/nwpac.html>) is a data assimilative model solution using the Estimating the Circulation and Climate of the Ocean (ECCO) package (Stammer et al., 2002). The ECCO system enables four-dimensional variational assimilation (4D-Var) and is based on the MIT General Circulation Model (MITgcm; Marshall et al., 1997) and its automatically derived adjoint model through Transformation of Algorithms in Fortran (TAF; Giering and Kaminski, 1998). The state estimate covers the domain of 115°E to 170°E and 15°S to 27°N, with 1/6° (~18 km) horizontal resolution and 50 vertical z-levels that gradually increase

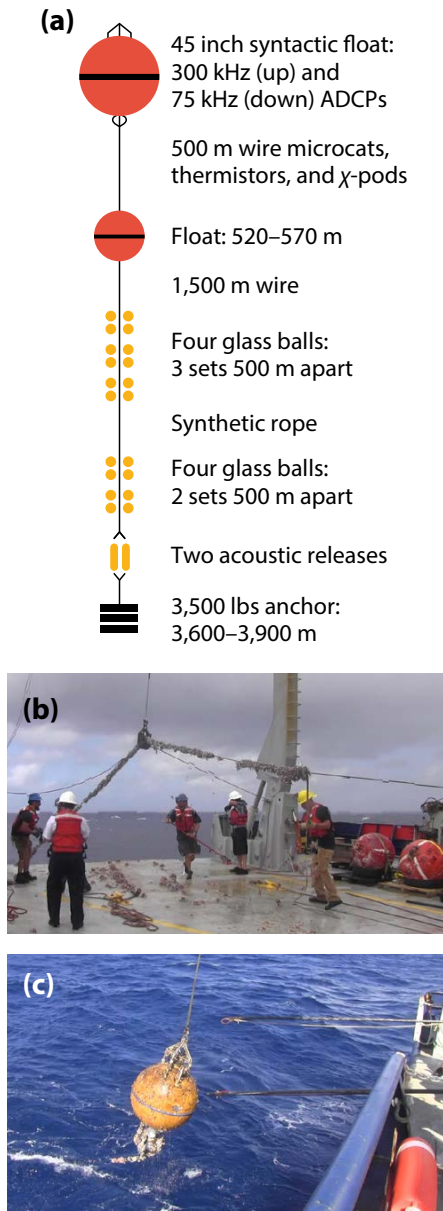


**FIGURE 3.** (a) Schematic of a deep subsurface ADCP mooring, with upward and downward ADCPs as described in Table 1. Temperature and velocity observations from the moorings are used here. (b,c) Mooring ball recovery from R/V Revelle in spring 2016. All were covered by biological growth.

**TABLE 1.** Deep, subsurface acoustic Doppler current profiler (ADCP) moorings deployed during the FLEAT program: M1, M2, M3, M4, and M5. The 300 kHz and 75 kHz ADCPs were mounted in a subsurface buoy at a depth of about  $Z_B$ . The 300 kHz ADCPs were upward looking and the 75 kHz ADCPs were downward looking.  $H$  is the water depth,  $\Delta t$  is the sampling period of the ADCPs, and  $\Delta z$  is the bin size.  $Z_B$  is the mean depth of the ADCP buoy from the surface. The depths of first and last bins of a given ADCP varied due to the movement of the mooring, and the ADCP velocity profiles were interpolated between  $Z_1$  and  $Z_n$  depth levels.

Site	Date	Latitude	Longitude	H (m)	$Z_B$ (m)	$Z_1$ (m)	$Z_n$ (m)	Type (kHz)	$\Delta t$ (min)	$\Delta z$ (m)
M1	05/24/16–04/04/17	8.438°N	134.431°E	2,600	64	8	600	Downward: 75	60	8
								Upward: 300	20	4
M2	05/21/16–03/31/17	8.258°N	134.794°E	2,610	80	8	600	Downward: 75	60	8
								Upward: 300	20	4
M3	05/23/16–04/03/17	8.618°N	134.487°E	2,846	66	8	600	Downward: 75	60	8
								Upward: 300	20	4
M4	05/22/16–04/02/17	8.605°N	134.602°E	1,350	91	8	600	Downward: 75	60	8
								Upward: 300	20	4
M5	05/21/16–04/01/17	8.523°N	134.871°E	3,610	73	8	600	Downward: 75	60	8
								Upward: 300	20	4

in spacing from the surface to the ocean floor. Ocean observations within the region 122°E to 170°E and 5°N to 20°N were assimilated into the model. Assimilated observations include CTD temperature and salinity data from glider and Argo floats (<http://www.argo.ucsd.edu>, <http://argo.jcommops.org>), temperature data from expendable bathythermographs (XBTs), and satellite-derived SSHA and SST. For the first-guess simulation of the state estimate, the initial and open-ocean boundary conditions are obtained from the data assimilative Navy Operational Hybrid Coordinate Ocean Model solutions using the Navy Coupled Ocean Data Assimilation (HYCOM+NCODA 1/12° global daily analysis; Chassignet et al., 2003; Halliwell, 2004; Cummings, 2005; Cummings and Smedstad, 2013), and the atmospheric forcing is obtained from National Centers for Environmental Prediction/National Center for Atmospheric Research (NCEP/NCAR) reanalysis (Kalnay et al., 1996). The adjoint-based MITgcm-ECCO 4D-Var assimilative method is used to adjust the model control variables (temperature and salinity initial conditions, open-ocean boundary conditions, and atmospheric forcing) to minimize the misfit between the first-guess simulation and ocean observations; it follows an iterative optimization procedure via a variable-storage Quasi-Newton M1QN3 algorithm (Gilbert and Lemaréchal, 1989). The optimized ocean state is a free running model solution that is forced using adjusted model controls and that conserves heat, salt, mass, and momentum over an assimilation window of four months before it is reinitialized from HYCOM/NCODA. The WPOSE was produced for the period 2009–2017 by merging optimized solutions from 27 estimates, each four months long. Output is archived in daily averages of the model state. For this study, 10-day averages of daily output are compared to observations. The WPOSE has been cross-validated and used in other western Pacific Ocean studies (Lien et al., 2015; Qiu et al., 2015; Schönau et al., 2015).

## A BASIN-WIDE TRANSITION

The 2015/16 El Niño peaked in strength from October 2015 to January 2016 (<https://www.cpc.ncep.noaa.gov/>) and was characterized by exceptionally large positive SST anomalies (SSTAs;  $\sim 2^{\circ}\text{C}$ ) and positive SSHAs ( $\sim 0.4\text{ m}$ ) in the eastern equatorial Pacific. The January 2016 SSTA (Figure 4a), obtained by subtracting the long-term annual cycle (1993–2017) from the monthly SST, and the

January 1, 2016, SSHA (Figure 4c) have large, positive anomalies in the far eastern Pacific, with the maxima centered on the equator. Near Palau, there are negative anomalies, corresponding to low sea level and lower than average SST.

When the trade winds returned at the end of the 2015/16 El Niño, they were exceptionally strong, creating positive wind stress curl anomalies in the central Pacific from November 2015 to

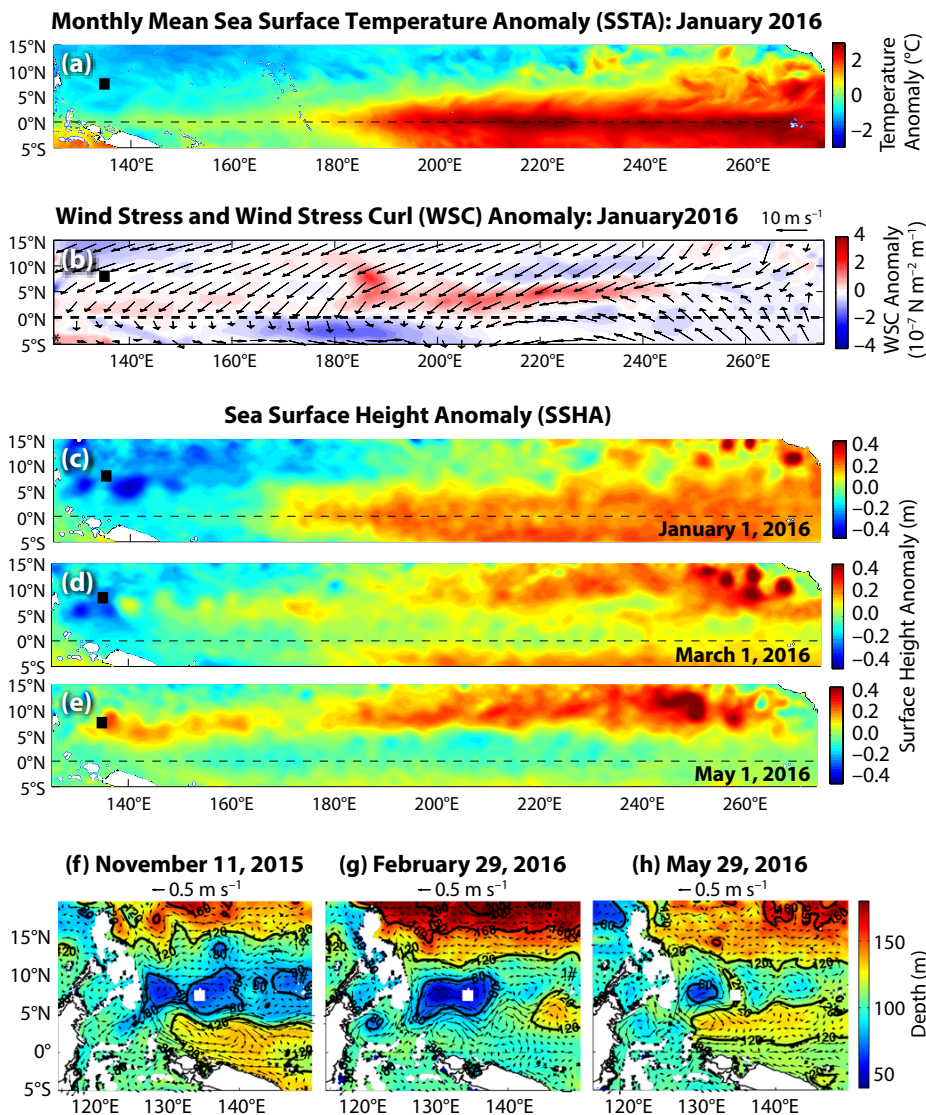


**FIGURE 4.** Conditions during and following the 2015/16 El Niño. (a) Monthly sea surface temperature anomaly (SSTA) (CMEMS reanalysis: GLORYS12V1) for January 2016 showing the anomalously warm eastern Pacific, characteristic of an El Niño. (b) Monthly wind vector and interannual wind stress curl anomaly (ECMWF) in January 2016 after the return of the trade winds. Sea surface height anomaly (SSHA) (CMEMS: AVISO/DUACS) in (c) January, (d) March, and (e) May 2016 during decay of the 2015/16 El Niño. Western Pacific Ocean State Estimate (WPOSE) mean upper ocean velocity and mean depth of the 21–26  $\text{kg m}^{-3}$  layer in (f) November 2015, (g) February 2016, and (h) May 2016 from 10-day averages of daily output. The North Equatorial Countercurrent is strong in November, and weakens with the arrival of Rossby waves, turning northward in February, with eastward flow disappearing by May 2016. The location of Palau is shown by black squares in (a–e) and white squares in (f–h).

April 2016. **Figure 4b** illustrates the strong northeasterlies that prevailed over the Pacific in January 2016. The trade winds redistribute the water zonally along the equator. In the off-equatorial tropical Pacific, Ekman pumping and suction forces long baroclinic Rossby waves that propagate westward owing to a need to conserve potential vorticity (Gill, 1982). The SSH variability is thus caused by wind forcing, either locally or remotely by the propagation of these planetary waves. In the central Pacific, the wind stress curl is positive between the equator and 8°N, which can induce an upwelling Rossby wave (decreasing SSH), and negative to the north of 8°N, yielding a downwelling wave (increasing SSH; **Figure 4b**). These waves propagate westward roughly by latitude, and their speeds increase with proximity to the equator. There is a lag time between the wind forcing over the central Pacific and the resulting dynamics near Palau. The decrease of the phase

speed with latitude further complicates how these signals arrive, affecting the meridional gradients in the thermocline that drive the geostrophic tropical circulation of the NEC and NECC. Evidence of this propagation is observed by changes in SSHA (**Figure 4c–e**); by March, the SSHAs have dissipated along the equator, while large, positive SSHAs moved westward in the northern Pacific and arrived near Palau in May 2016 (**Figure 4e**).

In the far western Pacific, there were changes in the mean depth of the upper ocean (from the surface to the base of the thermocline at 26 kg m<sup>-3</sup>) and in current velocities before and during the arrival of these anomalies, as shown by WPOSE (**Figure 4f–h**). To the south of Palau, the NECC had anomalously strong velocity and large transport before and during the peak of the 2015/16 El Niño (recent work of authors Schönau, Rudnick, Gopalakrishnan, and Cornuelle, and Qiu). In November 2015, during the

peak of the El Niño, the NECC is a strong eastward flow between 2°N and 5°N (**Figure 4f**), aided by a large meridional gradient in the upper ocean layer, from the surface to the base of the thermocline. This upper ocean layer was shallow near Palau and deep near the equator, which supported an eastward geostrophic velocity. By February (**Figure 4g**), this meridional gradient disappeared; an upwelling Rossby wave had shoaled the region between the equator and 5°N while at Palau a shallow region remained. The NECC, a geostrophic current, began to flow northeast near Palau, west of 140°E, in response to the pressure gradients. By May 2016 (**Figure 4h**), the downwelling wave had arrived, flattening out the upper ocean layer depth in the entire region, leading to a “shut-off” of the NECC and anomalous circulation. This explanation is a bit simplistic, however, as there were also nonlinear interactions between the Rossby waves and the currents that created barotropic and baroclinic instability and precipitated the dynamical breakdown of the NECC (Qiu et al., 2019, in this issue).

Satellite observations of SSHA and the associated anomalous geostrophic current vectors show the space-time evolution of westward-moving waves and their arrival at Palau (**Figure 5**). In March 2016, the arrival of the first SSHA was observed west of 140°E (**Figure 5a,b**); it quickly created an anomalous current westward with speed of about 0.5 m s<sup>-1</sup> by the end of March and early April (**Figure 5c,d**). The leading edge of a wave with a positive SSHA intensified as it reached Palau in late April (**Figure 5e**). The resulting flow field generated a strong northward flow to the east of Palau. Wave packets passed through the Palau island/reef area in May, with part of the incoming flow appearing to be reflected toward the northwest, and the resulting flow pattern showing anomalous northward flow to the west of Palau (**Figure 5f,g**). On June 7, a train of positive and negative SSHAs propagated westward south of Palau, and then dissipated by the end of June (**Figure 5i,j**).

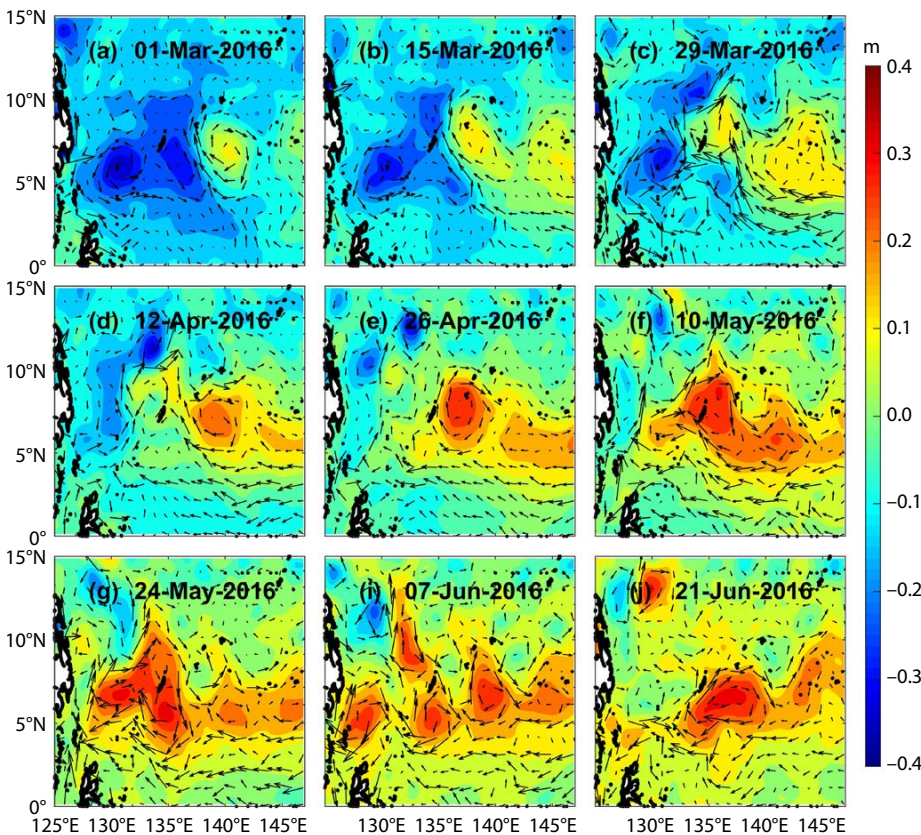


**FIGURE 5.** Longitude-latitude plots of SSHA (in m) for the transition period of El Niño to normal conditions in the western equatorial Pacific encompassing Palau (134.65°E, 8.5°N). Arrows are geostrophic velocities derived from the merged AVISO/DUACS product available from CMEMS.

Energy from incident SSHAs was dissipated as they encountered topography, through the creation of an island wake, lee waves, and smaller-scale turbulence near Palau, processes described elsewhere in this issue by Johnston et al., Rudnick et al., and St. Laurent et al. Spatial separation between two consecutive positive anomalies, which is roughly the zonal wavelength, was about 550 km. The arrival of the SSHAs corresponded to depth variability of the thermocline that was observed near Palau.

### A TRANSITION AT PALAU

Gliders, vertical temperature logger arrays, and moorings observed the arrival of the SSHAs at Palau. Data from the gliders and temperature loggers, which were in place during the arrival of the first of the SSHAs in March 2016, show the deepening of the thermocline and some of the spatial variability around Palau. Mooring observations, which began in May 2016, captured high-frequency observations of currents and hydrography during the adjustment phase following the El Niño, two months after the arrival of the warm water. The mooring data revealed the arrival of intraseasonal oscillations (ISOs) with periods of ~30 days that were consistent with the incoming wave field observed by satellites. There were strong northward currents and residual adjustments in the entire year following the event.

### Temperature and Salinity

Time series of glider potential temperature (Figure 6b) and salinity (Figure 6c) from October 2015 to January 2018 indicate a rapid change in the thermocline depth in March 2016. A seven-day running mean was applied to the glider time series to filter out high-frequency variability caused by the action of internal waves on the glider (Rudnick and Cole, 2011). Between mid-March and mid-April 2016, the 20°C isotherm, used as a proxy for thermocline depth across the tropical Pacific, deepened from 60 m to 120 m, reaching a maximum depth of

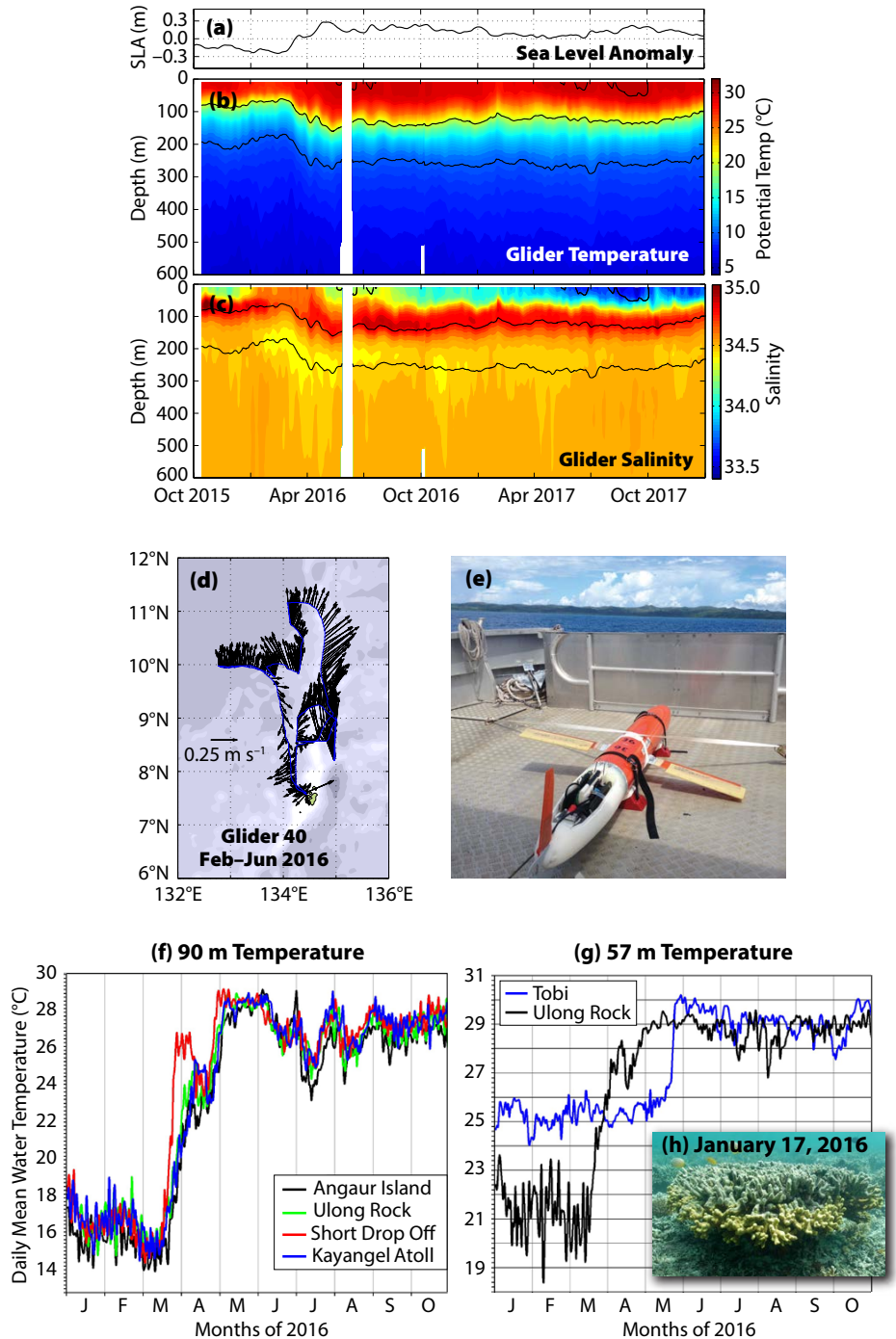


**FIGURE 6.** (a) Sea level anomaly (SLA) (CEEMS; three-day running mean) at 7.375°N, 134.375°E near Palau. Cross sections of (b) potential temperature and (c) salinity from gliders deployed during FLEAT. A seven-day running mean was applied to glider observations to minimize high-frequency internal wave motion. Data are drawn from 15 gliders, whose trajectories are shown in Figure 1a (pink). Black lines indicate the 10°C, 20°C, and 30°C isotherms. Changes in SLA correspond to a deepening of the thermocline (20°C isotherm) in late March 2016 as the basin-wide signals arrive at Palau. (d) Glider depth-average velocity of Glider 40, based on dead-reckoning, that was deployed from February 15 to June 6, 2016, during the transition from El Niño to normal conditions. Strong northward velocities near Palau concur with WPOSE results and mooring observations. (e) A glider ready for deployment in July 2016 aboard the catamaran *Kemeduki*. (f) Temperature logger observations on either side of the main island of Palau showing the change in temperature at 90 m depth near the reef in late March 2016. (g) A comparison of temperature at 57 m depth between Ulong Rock (7.3°N, 134.24°E) on the western side of the main island of Palau and Tobi (3°N and 131.1°E) (see Figure 1a). (h) A colony of a branching species of *Porites* coral on a very shallow reef flat on the main island group of Palau. The uppermost region of the colony was killed by mean low sea level through aerial exposure in late 2015. The flat-topped area of dead branches indicates the level to which earlier higher sea levels allowed the colony to grow.

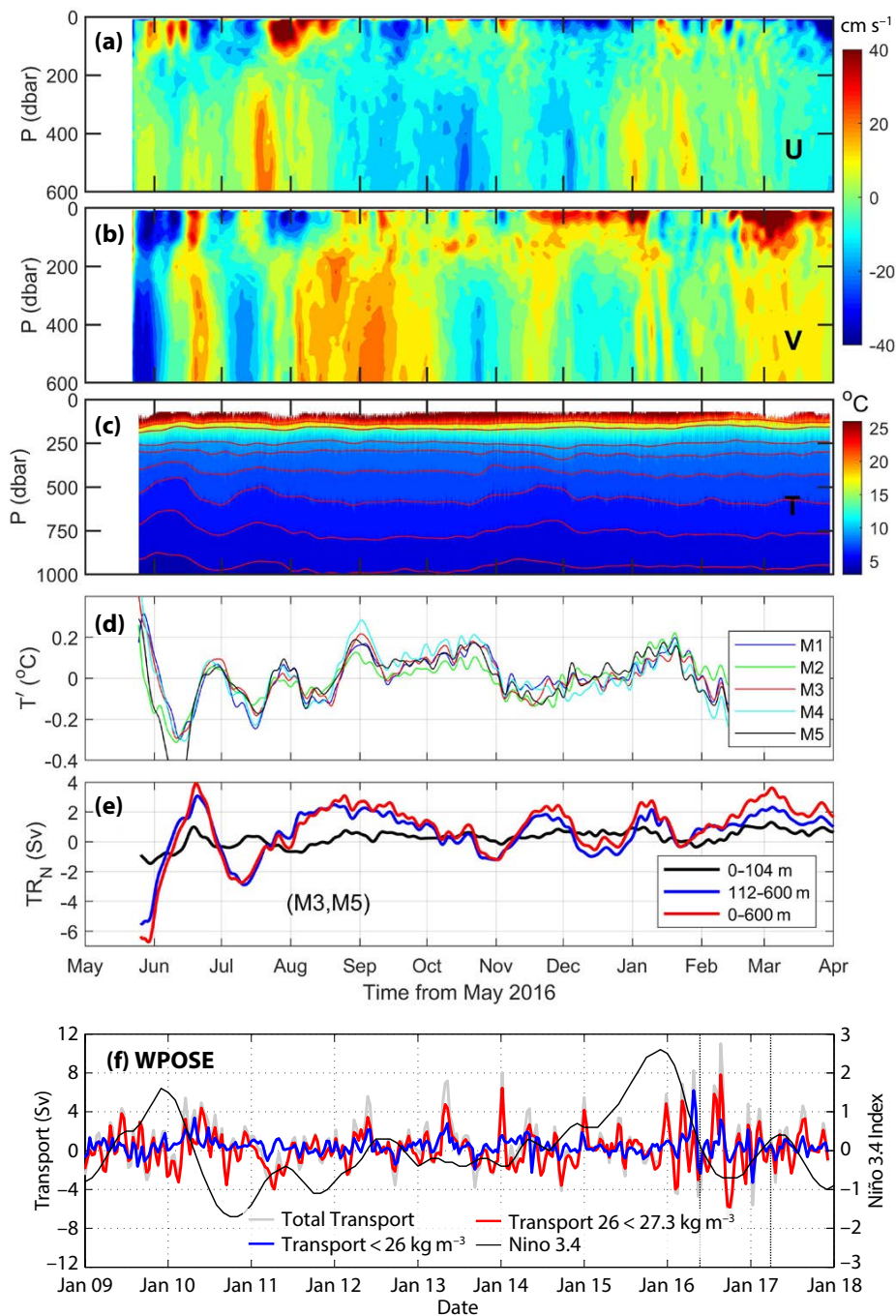


**FIGURE 7.** Ten-day low-pass-filtered data from the M5 mooring (see Figure 1b) for (a) the zonal (U) and (b) meridional (V) currents, and (c) temperature. The red lines in (c) are 5°C, 6°C, 7°C, 8°C, 9°C, 10°C, 15°C, 20°C, and 25°C isotherms, bottom to top, respectively. (d) Low-frequency temperature fluctuations from moorings M1–M5, estimated by subtracting the time mean from the depth-averaged (150–1,000 m), 10-day, low-pass-filtered temperature (T). (e) Meridional transports between the surface and 104 m, between 112 m and 600 m, and between the surface and 600 m, computed between moorings M3 and M5. Velocities are in  $\text{cm s}^{-1}$  and transport is in Sv ( $1 \text{ Sv} = 10^6 \text{ m}^3 \text{ s}^{-1}$ ). (f) Meridional transport from WPOSE at  $8.5^\circ\text{N}$ , integrated between nearest model grid-point pairs to mooring locations, plotted together with the Niño 3.4 index. Integration of the upper layer is from the surface to  $26 \text{ kg m}^{-3}$  (the base of the thermocline,  $\sim 200 \text{ m}$  depth), that of the lower layer is from the base of the thermocline to  $27.3 \text{ kg m}^{-3}$  ( $\sim 1,000 \text{ m}$  depth). The largest transports occur following the peak of the 2015/16 El Niño, with large oscillations near Palau for the entire year following. The vertical dashed lines indicate the beginning and end of the mooring transport time series (f).

160 m by the end of May, before settling to an average depth of 135 m. The transition was not smooth, with oscillations of 30 m to 45 m lasting up to two weeks, either caused by changes in glider location or incoming intraseasonal anomalies. By comparison, the standard deviation of the depth of the 20°C isotherm from June 2016 to January 2018 was roughly 20 m, much less than the depth change associated with the end of the El Niño transition. The change in thermocline corresponded to similar timing in the shift in sea level anomaly at Palau (Figure 6a) and observations from the temperature logger arrays on either side of Palau. The temperature at 90 m depth changed from near 16°C in March to 28°C at the end of May (Figure 6f). These changes coincide with the arrival of SSHAs in mid-March through May (Figures 4 and 5). It is interesting to observe that there was a quicker, more extreme response at Short Drop Off, on the eastern side of the main Palau island group, than at the measurement locations on the north, west, and south sides. This warm anomaly lasted a few weeks before synchronizing with the other stations. The spatial variability in temperature and arrival times of signals evident in WPOSE and satellite observations is shown in greater detail by comparison of the temperature at Ulong Rock, on Palau’s western reef, to the temperature at Tobi, roughly 600 km to the southwest of Palau’s main island group (Figure 6g). The temperature extremes during the El Niño were less at Tobi than at the main Palau group. At Tobi, the downwelling wave arrived later in May, and the change in temperature at 57 m depth was nearly half of that at Ulong rock at 57 m depth.

Following their deployment in late May, the moorings recorded vertical displacements of isotherms exceeding 100 m in the deeper part of thermocline (Figure 7c). The temperature fluctuations show 30-day oscillations that lasted until the middle of September at all mooring sites (Figure 7d). Temperature fluctuations at each mooring were computed by

first creating a depth-average of temperatures below 150 m, and then subtracting the time mean. The phase coincided with shallower monthly oscillations from May to August at 90 m in the vertical temperature logger array (Figure 6f). By the end of 2016, the gliders observed fresh surface water near Palau (Figure 6c), which is characteristic of precipitation and advection from the warm pool, and the intraseasonal oscillations that immediately followed the El Niño became indistinguishable.

### Velocity and Transport

The depth-averaged velocity from a glider that was deployed in February 2016 and profiled until June 2016 captured the strong, variable currents near Palau during the transition from El Niño to normal conditions (Figure 6d). The glider was sent to profile on the eastern side of Palau's northern reef and was quickly caught in a strong northeastward flow that was too powerful for the glider to overcome. The flow at 9°N is typically westward in the NEC, although eastward velocity was also observed at that latitude in June 2010 following the 2009/10 El Niño (Figure 6a in Schönau and Rudnick, 2015). The erratic currents from the glider verify the anomalous circulation from WPOSE (Figure 4) and satellite observations (Figure 5) as the region adjusted to normal conditions.

The moorings were deployed in May, after the deepening of the thermocline observed by the gliders, and the occurrence of some of the erratic northeastward velocities. Immediately following the end of the El Niño, intraseasonal oscillations were visible in the meridional velocity of the moorings, with magnitudes as large as  $0.4 \text{ m s}^{-1}$  (Figure 7b). There was greater variability in zonal velocities during this period as well (Figure 7a). The strong velocity anomalies in summer 2016 were in phase with the deep shifts in isotherms (Figure 7c).

The deep oscillations were associated with changes in transport, which can be computed between the moorings.

Transports were calculated between 0 m and 104 m, 112 m and 600 m, and 0 m and 600 m to look at the vertical structure. Zonal transport, computed between M1 and M3, and between M2 and M5, were typically less than about 1.5 Sv. This may be expected as the island and reef block most of the zonal flow. Variability in total (0–600 m) meridional transports was greater, ranging from  $-6 \text{ Sv}$  to  $4 \text{ Sv}$ , and was greatest immediately after the termination of El Niño (Figure 7e). Variability in meridional transport after the transition period was generally less than 2 Sv.

It is difficult to determine from the one-year time series what the typical northward transport may be near Palau, so a comparison to the longer-transport time series from WPOSE is insightful (Figure 7f). From January 2009 to December 2017, the mean northward transport was  $0.6 \text{ Sv}$ , with an annual cycle falling within a  $2.5 \text{ Sv}$  range. Similar to the mooring results, the transport below the thermocline contributed the most to total transport. The maximum transports were observed during the adjustment following the 2015/16 El Niño conditions, with total northward transports exceeding  $8 \text{ Sv}$ . The slightly greater transports in WPOSE likely arise from a greater longitudinal distance between model grid points ( $0.5^\circ$ ) than between the moorings ( $0.38^\circ$ ). However, the pattern, if not the phase, in 2016 from spring to fall is roughly the same as the moorings observed, with transport fluctuations during the adjustment having a period of 30 days. WPOSE shows that the meridional transport variability was greatest during the adjustment from the 2015/16 El Niño than at any period in the previous decade.

### DISCUSSION

The sudden changes in thermocline depth and the arrival of intraseasonal current and SSH anomalies were apparent in observations and model results during the end stages of the 2015/16 El Niño and the transition that followed. Some important points not considered

in the analysis above are the relationship of these changes to the annual cycle, the sources of these oscillations and whether they are typical at the termination of El Niño events, and the impact that the transition from El Niño to normal conditions may have for Palau's coral reefs.

The annual cycle in the region surrounding Palau is influenced by a change in wind forcing. Typically, the convergence of the northeast and southeast trade winds in the Intertropical Convergence Zone (ITCZ) is south of the equator in January, with strong northeasterlies over the northern tropical Pacific. This leads to the upwelling around Palau known as the Mindanao Dome and recirculation between the NECC, NEC, and MC in spring (Masumoto and Yamagata, 1991). In summer, an annual downwelling Rossby wave generated in the central Pacific arrives, the wind changes to southwesterlies over the region, and the thermocline deepens. There is also increased precipitation as the ITCZ moves over the region. There is a relationship between the annual cycle of wind forcing over the tropical Pacific and eastern Asia and the interannual phenomena of ENSO. An El Niño typically develops from April to November (Clarke, 2014), and its decay is in phase with the reappearance of the trade winds across the Pacific that occurs from November to December and persists through April. The annual and interannual phenomena are so linked that some investigators have looked at ENSO as an interaction between an annual and an interannual mode (Tozuka et al., 2003). Thus, the anomalies that were observed near Palau are caused by a return of normal conditions and are in phase with the seasonal cycle. During spring, it is expected that the NECC will turn northward, as it did in 2016, as part of the recirculation of the Mindanao Dome, and that the thermocline will be shallow and then deepen from April through June. Some of the thermocline adjustment and current anomalies in 2016 may have been related to this annual cycle, which is difficult to

remove given the length of our observations. However, it appears from satellite observations, WPOSE, and a decade of glider observations that the anomalies in 2016, during the adjustment to normal conditions, exceed those that would occur annually. The annual thermocline displacement tends to be much less, and although the NECC tends to recirculate some in the spring, it doesn't typically stop flowing eastward.

Our analysis found that intraseasonal oscillations with a phase speed characteristic of Rossby waves in the western equatorial Pacific occur near Palau during the transition of El Niño to ENSO neutral conditions. In 2016, wave characteristics were estimated from SSHAs and moored current and temperature observations. Wave period, phase speed, and zonal wavelength were 30 days,  $0.2 \text{ m s}^{-1}$ , and 550 km, respectively. To examine the

existence of these waves during other major El Niño events, we examined weekly averaged SSHAs across the Pacific Ocean from 1993 to 2017. SSHAs were first low-pass filtered ( $\eta_{120L}$ ) to examine seasonal variability (Figure 8a) and then were high-pass filtered ( $\eta_{120H}$ ) to capture intraseasonal variability (Figure 8b). Several major ENSO events can be easily identified during different time periods from large negative SSHA values in the western Pacific (Figure 8a). Major events occurred in 1997/98 and 2015/16, while events in 2002/03, 2006/07, and 2009/10 were moderate. The transition from El Niño to ENSO-neutral or La Niña is often associated with a large increase of  $\langle(\eta_{120H})^2\rangle$  in the western equatorial Pacific, especially for the 1997/98, 2002/03, and 2015/16 events (Figure 8b). Here,  $\langle(\eta_{120H})^2\rangle$  was averaged over a  $10^\circ$  longitudinal band between  $131.125^\circ\text{E}$

and  $141.124^\circ\text{E}$  to obtain  $\langle(\eta_{120H})^2\rangle$ . These three events also had the greatest variability in low frequency SSH.

To examine these three El Niño events, Figure 9 shows time-longitude plots of 120-day high-pass-filtered SSHAs in the western Pacific ( $125^\circ\text{E}$ – $150^\circ\text{E}$ ) at three different latitudes ( $7.625^\circ\text{N}$ ,  $8.625^\circ\text{N}$ ,  $9.625^\circ\text{N}$ ) for each event. Westward-propagating waves were observed during 2016, 2003, and 1998 (Figure 9a–c). The slopes of the time-longitude plots indicate that waves propagated westward with phase speeds of about  $0.2 \text{ m s}^{-1}$  at  $8.625^\circ\text{N}$ , within phase speed ranges of mode-1 and mode-2 linear baroclinic Rossby waves. These intraseasonal oscillations appear to be localized to the west of the date line, unlike low-frequency Rossby waves that can span the Pacific basin and gain strength near Palau. Thus, the adjustment around Palau that occurred following the 2015/16 El Niño may have also occurred during the transition from previous El Niño events. The source of the waves may be anomalously strong wind stress curl in the central tropical Pacific that occurred with the return of the trade winds (e.g., Figure 4b). In January of each end of El Niño year (i.e., 1998, 2003, 2010, 2016), there were exceptionally strong, positive wind stress curl interannual anomalies between  $160^\circ\text{E}$  and  $240^\circ\text{E}$ , and  $0^\circ$  and  $10^\circ\text{N}$ ; the strongest anomalies occurred in 1998 and 2016. However, in 2016, these waves did not appear to have propagated from east of  $150^\circ\text{E}$  but rather had a more local source, either from current instability or local wind stress curl anomalies.

Oscillations that propagate westward need not be Rossby waves because near the equator, the equatorial waveguide can cause both mixed Rossby-gravity (MRG) waves and tropical instability waves (TIWs) to form. MRG waves typically have some symmetry about the equator, with their amplitude greatest between  $5^\circ\text{S}$  and  $5^\circ\text{N}$  (Farrar and Durland, 2012). However, the amplitudes of the observed intraseasonal oscillations were greatest away from the equator, from  $5^\circ\text{N}$  to  $11^\circ\text{N}$ ,

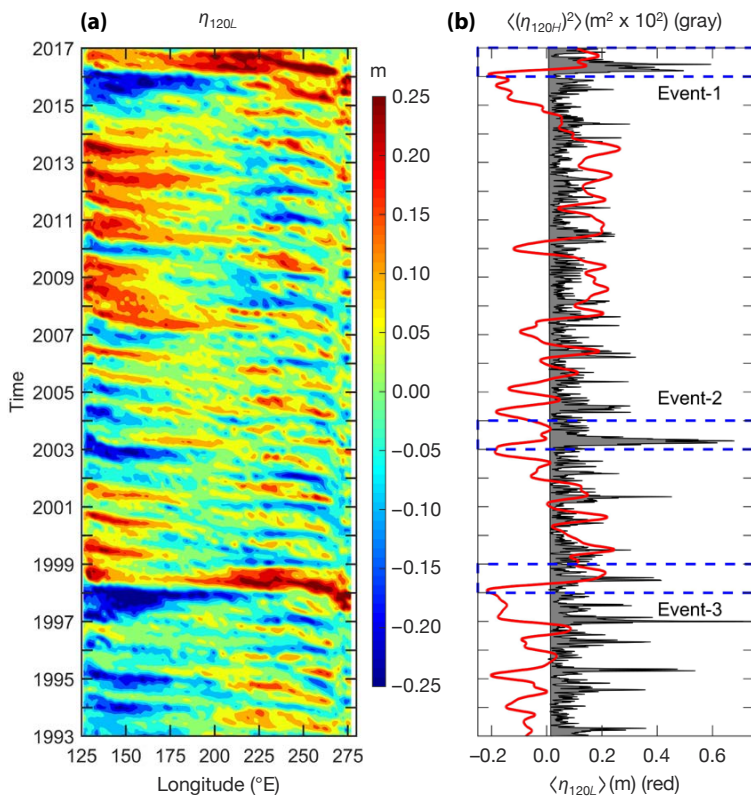


**FIGURE 8.** Sea surface height anomaly (SSHA) from AVISO/DUACS. (a) 120-day low-pass-filtered SSHA ( $\eta_{120L}$ ) plotted as a Hovmöller diagram along  $8.625^\circ\text{N}$  across the Pacific between January 1993 and July 2017. (b) 120-day low-pass-filtered SSHA (thick red line) and squared 120-day high-pass-filtered SSHA,  $\langle(\eta_{120H})^2\rangle$  (filled gray area) averaged between  $131.125^\circ\text{E}$  and  $141.125^\circ\text{E}$ . SSHA is in meters. Horizontal dashed lines indicate the termination of El Niño events shown in greater detail in Figure 7 (Event-1: 2016, Event-2: 2003, and Event-3: 1998).

and we found no evidence of them in the Southern Hemisphere, making it unlikely that they are examples of MRG waves. It is also uncertain that TIWs, typical of the eastern and central Pacific (Chelton et al., 2000), would be this strong at a relatively high latitude and far western location. For these reasons, we believe the intraseasonal SSHAs to be Rossby waves.

It is worth noting that while 1997/98 and 2015/16 were considered to be eastern Pacific El Niños by their large SSTs in the Niño 3.4 region, the 2002/03 event was a central Pacific El Niño with a different spatial pattern (Santoso et al., 2019). Furthermore, the El Niño event in 2009/10 had a higher value on the Niño 3.4 index, a similar wind stress curl anomaly in January, and shoaling near Palau compared to the El Niño in 2002/03, but it did not have strong, intraseasonal variability as assessed by  $\langle(\eta_{120H})^2\rangle$ . The 2009/10 El Niño also did not have strong meridional transport anomalies (Figure 7f) compared to those in 2015/16. This discrepancy reinforces the idea that each El Niño is unique and that its impact on a particular region, such as near Palau, cannot be easily reduced to a single index.

It is interesting to consider how the intraseasonal waves that accompany the termination of an El Niño event, which deepen the thermocline and cause current variability, may impact Palau's coral reefs. Immediately following the 2015/16 El Niño, currents changed near Palau—for example, the NECC disappeared and northward flow appeared—which may affect nutrient availability and salinity near Palau. Thermocline depth variability during and following the El Niño can result in large temperature variability and nutrient flux at depths where coral grows. For instance, there is evidence that shallower thermoclines during El Niño may lead to phytoplankton blooms at mesophotic reef depths (Colin, 2018). Some mesophotic reefs have corals growing to 150 m depth; however, in Palau, they are limited to about 60 m to 75 m depth, potentially with temperature being the depth-limiting factor rather than light.

The combination of a strong thermocline and internal wave motion can alter the temperature up to 20°C at depths of 60 m to 120 m in 30 minutes (Wolanski et al., 2004). Thus, the mesophotic reef must be resilient to some level of short-period temperature variance. However, ENSO events create persistent thermal anomalies, either deepening or shoaling the thermocline, that can lead to coral bleaching from excessively warm or cold temperatures (Colin, 2018). Temperature variability can also be associated with water mass transport by eddies and nonlinear Rossby waves, both of which were observed in the region in 2016 during the end of El Niño (Andres et al., 2019, and Qiu et al., 2019, both in this issue). Die-off can also occur on shallow reefs during the mean low sea levels that persist during El Niño. Figure 6h shows a

photograph from January 2016 of *Porites* coral on a very shallow reef to the north of Palau. The uppermost part of the coral has dead branches caused by exposure during low sea level in late 2015.

The glider, temperature logger, and mooring observations illustrate how the transition from the relatively cold El Niño conditions to normal conditions occurred in 2016. At a depth of 70 m to 90 m, the extreme lower depth limits of coral growth near Palau, the temperature in March 2016 was 16°C to 18°C. During the transition from El Niño to normal conditions, the temperature saw-sawed upward, rising quickly, stabilizing for a few weeks, decreasing slightly, and then making another jump. By the end of May, the temperatures in this depth range were near 29°C, so high that there was a risk of coral bleaching. Cooling arrived

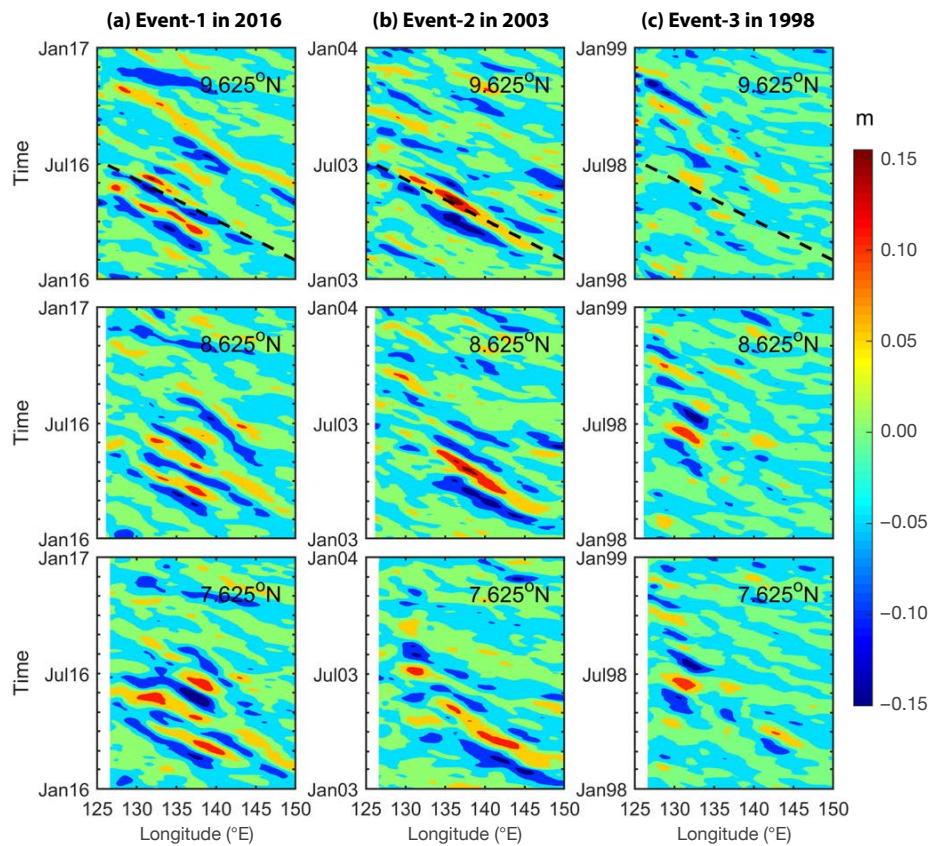


**FIGURE 9.** 120-day high-pass-filtered SSHA ( $\eta_{120H}$ ) plotted in a Hovmöller diagram along 7.625°N (bottom row), 8.625°N (middle row), and 9.625°N (top row) showing intraseasonal oscillations after three major El Niño events: (a) Event-1 in 2016, (b) Event-2 in 2003, and (c) Event-3 in 1998. Units are in meters. The slope of a time-longitude plot is the phase speed of the westward moving wave, which is about 0.2 m s<sup>-1</sup> at 8.625°N. The phase speed line of 0.2 m s<sup>-1</sup> is shown as a dashed line for each event in the top panels.

by early June, and temperatures dropped to between 22°C and 26°C by the end of 2016, more consistent with the long-term mean. These observations verify that there is no deep “refuge” for mesophotic reefs during ENSO extremes, as also found by Colin (2018) and Schramek, et al. (2018), and confirm the importance of in situ measurements at depth when monitoring coral reef health.

The intraseasonal oscillations near Palau during and following the end of an El Niño may be beneficial to the coral reefs. Coral bleaching occurs during sustained thermal anomalies, but these effects can be lessened if the reef receives an influx of cold water from upwelling (Colin, 2018). In 2010, coral bleaching occurred following the 2009/10 El Niño as a La Niña materialized almost immediately; the lack of southwest monsoon formation led to sustained high temperatures in reef waters (Colin, 2018). However, bleaching did not occur in 2016 (Colin, 2018). Although temperatures approached 30°C at 70 m depth by the middle of June 2016, they decreased by early July as intraseasonal oscillations brought temporary upwelling and normal, seasonal winds soon prevailed over the region. The oscillatory nature of the temperature caused by the intraseasonal waves may have been helpful in temporarily relieving the thermal stress on the coral.

## SUMMARY

The oceanic response to the termination of a major El Niño event in 2015/16 was captured by in situ and satellite observations, and analyzed with a regional ocean state estimate near Palau as part of the FLEAT project. Negative (cold) SSHAs occupied the low-latitude western Pacific Ocean during 2015 and the early part of 2016. During the transition from El Niño to neutral conditions in spring 2016, pulses of positive (warm) SSHAs moved westward and reached Palau by the end of March. Arrival of these warm anomalies coincided with the disappearance of the eastward current flow associated with

the NECC. Nearly two months after the arrival of the warm water, intraseasonal oscillations in meridional velocity and vertical displacements of isotherms below the thermocline were observed that coincided with relatively large meridional transports near Palau. At the latitude of Palau, the SSHA data showed packets of westward-moving waves with phase speeds of about 0.2 m s<sup>-1</sup>, within the expected phase-speed ranges of mode-1 and mode-2 linear baroclinic Rossby waves. Similar SSHAs were found near Palau and over the Kyushu-Palau Ridge after major El Niño events, suggesting that intraseasonal oscillations are part of an oceanic response to the termination of El Niño. The magnitude of subsurface temperature anomalies during an El Niño event and the subsequent transition to neutral conditions can impact the health of the Palau’s coral reefs. 

## REFERENCES

- Andres, M., M. Siegelman, V. Hormann, R.C. Musgrave, S.T. Merrifield, D.L. Rudnick, M.A. Merrifield, M.H. Alford, G. Voet, H.W. Wijesekera, and others. 2019. Eddies, topography, and the abyssal flow by the Kyushu-Palau Ridge near Velasco Reef. *Oceanography* 32(4):46–55, <https://doi.org/10.5670/oceanog.2019.410>.
- Bruno, J.F., C.E. Siddon, J.D. Whitman, P.L. Colin, and M.A. Toscano. 2001. El Niño related coral bleaching in Palau, western Caroline Islands. *Coral Reefs* 20:127–136, <https://doi.org/10.1007/s003380100151>.
- Chassignet, E.P., L.T. Smith, G.R. Halliwell, and R. Bleck. 2003. North Atlantic simulations with the HYbrid Coordinate Ocean Model (HYCOM): Impact of the vertical coordinate choice, reference pressure, and thermobaricity. *Journal of Physical Oceanography* 33:2,504–2,526, [https://doi.org/10.1175/1520-0485\(2003\)033<2504:NASWTH>2.0.CO;2](https://doi.org/10.1175/1520-0485(2003)033<2504:NASWTH>2.0.CO;2).
- Chelton, D.B., F.J. Wentz, C.L. Gentemann, R.A. de Szoeke, and M.G. Schlax. 2000. Satellite microwave SST observations of transequatorial tropical instability waves. *Geophysical Research Letters* 27(9):1,239–1,242, <https://doi.org/10.1029/1999GL011047>.
- Clarke, A.J. 2014. El Niño physics and El Niño predictability. *Annual Review of Marine Science* 6:79–99, <https://doi.org/10.1146/annurev-marine-010213-135026>.
- Colin, P.L. 2009. *Marine Environments of Palau*. Indo-Pacific Press, 414 pp, <http://coralreefpalau.org/wp-content/uploads/2017/04/Colin-PL-2009-Marine-Environments-of-Palau.pdf>.
- Colin, P.L. 2018. Ocean warming and the reefs of Palau. *Oceanography* 31(2):126–135, <https://doi.org/10.5670/oceanog.2018.214>.
- Cummings, J.A. 2005. Operational multi-variate ocean data assimilation. *Quarterly Journal of the Royal Meteorological Society Part C* 131(613):3,583–3,604, <https://doi.org/10.1256/qj.05.105>.
- Cummings, J.A., and O.M. Smedstad. 2013. Variational data assimilation for the global ocean. Pp. 303–343 in *Data Assimilation for Atmospheric, Oceanic and Hydrologic Applications*, vol. II. S.K. Park and L. Xu, eds, Springer, [https://doi.org/10.1007/978-3-642-35088-7\\_13](https://doi.org/10.1007/978-3-642-35088-7_13).
- Dee, D.P., S.M. Uppala, J.A. Simmons, P. Berrisford, P. Poli, S. Kobayashi, U. Andrae, M.A. Balmaseda, G. Balsamo, P. Bauer, and others. 2011. The ERA-Interim reanalysis: Configuration and performance of the data assimilation system. *Quarterly Journal of the Royal Meteorological Society* 137:553–597, <https://doi.org/10.1002/qj.828>.
- Farrar, J.T., and T.S. Durland. 2012. Wavenumber-frequency spectra of inertia-gravity and mixed Rossby-gravity waves in the equatorial Pacific Ocean. *Journal of Physical Oceanography* 42:1,859–1,881, <https://doi.org/10.1175/JPO-D-11-0235.1>.
- Giering, R., and T. Kaminski. 1998. Recipes for adjoint code construction. *ACM Transactions on Mathematical Software* 24(4):437–474, <https://doi.org/10.1145/293686.293695>.
- Gilbert, J., and C. Lemaréchal. 1989. Some numerical experiments with variable-storage quasi-Newton algorithms. *Mathematical Programming* 45(1):407–435, <https://doi.org/10.1007/BF01589113>.
- Gill, Adrian E. 1982. *Atmosphere-Ocean Dynamics*. Academic Press, New York, 662 pp.
- Hacker, P., E. Firing, R. Lukas, P.L. Richardson, and C.A. Collins. 1989. Observations of the low-latitude western boundary circulation in the Pacific during WEPOCS III. Pp. 135–143 in *Proceedings of the Western Pacific International Meeting and Workshop on TOGA COARE*, Nouméa, New Caledonia, Institut Français de Recherche Scientifique pour le Développement en Coopération/Centre ORSTOM.
- Halliwell, G.R. 2004. Evaluation of vertical coordinate and vertical mixing algorithms in the HYbrid Coordinate Ocean Model (HYCOM). *Ocean Modelling* 7:285–322, <https://doi.org/10.1016/j.ocemod.2003.10.002>.
- Hsin, Y.-C., and B. Qiu. 2012. The impact of Eastern-Pacific versus Central-Pacific El Niños on the North Equatorial Countercurrent in the Pacific Ocean. *Journal of Geophysical Research* 117(C11), <https://doi.org/10.1029/2012JC008362>.
- Hu, D.X., L. Wu, W. Cai, A. Sen Gupta, A. Ganachaud, B. Qiu, A.L. Gordon, X. Lin, Z. Chen, S. Hu, and others. 2015. Pacific western boundary currents and their roles in climate. *Nature* 522:299–308, <https://doi.org/10.1038/nature14504>.
- Jacox, M.G., E.L. Hazen, K.D. Zaba, D.L. Rudnick, C.A. Edwards, A.M. Moore, and S.J. Bograd. 2016. Impacts of the 2015–2016 El Niño on the California Current System: Early assessment and comparison to past events. *Geophysical Research Letters* 43:7,072–7,080, <https://doi.org/10.1002/2016GL069716>.
- Johnston, T.M.S., J.A. MacKinnon, P.L. Colin, P.J. Haley Jr., P.F.J. Lermusiaux, A.J. Lucas, M.A. Merrifield, S.T. Merrifield, C. Mirabito, J.D. Nash, and others. 2019. Energy and momentum lost to wake eddies and lee waves generated by the North Equatorial Current and tidal flows at Peleliu, Palau. *Oceanography* 32(4):110–125, <https://doi.org/10.5670/oceanog.2019.417>.
- Kalnay, E., M. Kanamitsu, R. Kistler, W. Collins, D. Deaven, L. Gandin, M. Iredell, S. Saha, G. White, J. Woollen, and others. 1996. The NCEP/NCAR 40-year reanalysis project. *Bulletin of the American Meteorological Society* 77(3):437–471, [https://doi.org/10.1175/1520-0477\(1996\)077<0437:TNYRP>2.0.CO;2](https://doi.org/10.1175/1520-0477(1996)077<0437:TNYRP>2.0.CO;2).

- Kashino, Y., A. Atmadipoera, Y. Kuroda, and Lukijanto. 2013. Observed features of the Halmahera and Mindanao eddies. *Journal of Geophysical Research* 118:6,543–6,560, <https://doi.org/10.1002/2013JC009207>.
- L'Heureux, M.L., K. Takahashi, A.B. Watkins, A.G. Barnston, E.J. Becker, T.E. Diliberto, F. Gamble, J. Gottschalck, M.S. Halpert, B. Huang, and others. 2017. Observing and predicting the 2015/16 El Niño. *Bulletin of the American Meteorological Society* 98(7):1,363–1,382, <https://doi.org/10.1175/BAMS-D-16-0009.1>.
- Lien, R.-C., B. Ma, C.M. Lee, T.B. Sanford, V. Mensah, L.R. Centurioni, B.D. Cornuelle, G. Gopalakrishnan, A.L. Gordon, M.-H. Chang, and others. 2015. The Kuroshio and Luzon Undercurrent east of Luzon Island. *Oceanography* 28(4):54–63, <https://doi.org/10.5670/oceanog.2015.81>.
- Marshall, J., A. Adcroft, L. Perelman, and C. Heisey. 1997. A finite-volume, incompressible Navier Stokes model for studies of the ocean on parallel computers. *Journal of Geophysical Research* 102:5,753–5,766, <https://doi.org/10.1029/96JC02775>.
- Masumoto, Y., and T. Yamagata. 1991. Response of the western tropical Pacific to the Asian winter monsoon: The generation of the Mindanao Dome. *Journal of Physical Oceanography* 21:1,386–1,398, [https://doi.org/10.1175/1520-0485\(1991\)021<1386:ROTWTP>2.0.CO;2](https://doi.org/10.1175/1520-0485(1991)021<1386:ROTWTP>2.0.CO;2).
- McPhaden, M.J., A.J. Busalacchi, R. Cheney, J.-R. Donguy, K.S. Gage, D. Halpern, M. Ji, P. Julian, G. Meyers, G.T. Mitchum, and others. 1998. The Tropical Ocean-Global Atmosphere observing system: A decade of progress. *Journal of Geophysical Research* 103(C7):14,169–14,240, <https://doi.org/10.1029/97JC02906>.
- McPhaden, M.J. 1999. Genesis and evolution of the 1997–98 El Niño. *Science* 283:950–954, <https://doi.org/10.1126/science.283.5404.950>.
- McPhaden, M.J. 2008. Evolution of the 2006–2007 El Niño: The role of intraseasonal to interannual time scale dynamics. *Advances in Geoscience* 14:219–230, <https://doi.org/10.5194/adgeo-14-219-2008>.
- Meyers, G., P. McIntosh, L. Pigot, and M. Pook. 2007. The years of El Niño, La Niña, and interactions with the tropical Indian Ocean. *Journal of Climate* 20:2,872–2,880, <https://doi.org/10.1175/JCLI4152.1>.
- Qiu, B., D.L. Rudnick, S. Chen, and Y. Kashino. 2013. Quasi-stationary North Equatorial Undercurrent jets across the tropical North Pacific Ocean. *Geophysical Research Letters* 40:2,183–2,187, <https://doi.org/10.1002/grl.50394>.
- Qiu, B., D.L. Rudnick, I. Cerovecki, B.D. Cornuelle, S. Chen, M.C. Schönau, J.L. McClean, and G. Gopalakrishnan. 2015. The Pacific North Equatorial Current: New insights from the Origins of the Kuroshio and Mindanao Currents (OKMC) Project. *Oceanography* 28(4):24–33, <https://doi.org/10.5670/oceanog.2015.78>.
- Qiu, B., S. Chen, B.S. Powell, P.L. Colin, D.L. Rudnick, and M.C. Schönau. 2019. Nonlinear short-term upper ocean circulation variability in the tropical western Pacific. *Oceanography* 32(4):22–31, <https://doi.org/10.5670/oceanog.2019.408>.
- Rudnick, D.L., R.E. Davis, C.C. Eriksen, D.M. Fratantoni, and M.J. Perry. 2004. Underwater gliders for ocean research. *Marine Technology Society Journal* 38:73–84, <https://doi.org/10.4031/002533204787522703>.
- Rudnick, D.L., and S.T. Cole. 2011. On sampling the ocean using underwater gliders. *Journal of Geophysical Research* 116, C08010, <https://doi.org/10.1029/2010JC006849>.
- Rudnick, D.L., S. Jan, and C.M. Lee. 2015. A new look at circulation in the western North Pacific. *Oceanography* 28(4):16–23, <https://doi.org/10.5670/oceanog.2015.77>.
- Rudnick, D.L., K.L. Zeiden, C.Y. Ou, T.M.S. Johnston, J.A. MacKinnon, M.H. Alford, and G. Voet. 2019. Understanding vorticity caused by flow passing an island. *Oceanography* 32(4):66–73, <https://doi.org/10.5670/oceanog.2019.412>.
- Santoso, A., M.J. McPhaden, and W. Cai. 2017. The defining characteristics of ENSO extremes and the strong 2015/2016 El Niño. *Reviews of Geophysics* 55:1,079–1,129, <https://doi.org/10.1002/2017RG000560>.
- Santoso, A., H. Hendon, A. Watkins, S. Power, D. Dommenget, M.H. England, L. Frankcombe, N.J. Holbrook, R. Holmes, P. Hope, and others. 2019. Dynamics and predictability of El Niño–Southern Oscillation: An Australian perspective on progress and challenges. *Bulletin of the American Meteorological Society* 100:403–420, <https://doi.org/10.1175/BAMS-D-18-0057.1>.
- Schönau, M.C., and D.L. Rudnick. 2015. Glider observations of the North Equatorial Current in the western tropical Pacific. *Journal of Geophysical Research* 120:3,586–3,605, <https://doi.org/10.1002/2014JC010595>.
- Schönau, M.C., D.L. Rudnick, I. Cerovecki, G. Gopalakrishnan, B.D. Cornuelle, J.L. McClean, and B. Qiu. 2015. The Mindanao Current: Mean structure and connectivity. *Oceanography* 28(4):34–45, <https://doi.org/10.5670/oceanog.2015.79>.
- Schönau, M.C., and D.L. Rudnick. 2017. Mindanao Current and Undercurrent: Thermohaline structure and transport from repeat glider observations. *Journal of Physical Oceanography* 47:2,055–2,075, <https://doi.org/10.1175/JPO-D-16-0274.1>.
- Schramek, T.A., P.L. Colin, M.A. Merrifield, and E.J. Terrill. 2018. Depth-dependent thermal stress around corals in the tropical Pacific Ocean. *Geophysical Research Letters* 45(18):9,739–9,747, <https://doi.org/10.1029/2018GL078782>.
- Stammer, D., C. Wunsch, R. Giering, C. Eckert, P. Heimbach, J. Marotzke, A. Adcroft, C.N. Hill, and J. Marshall. 2002. Global ocean circulation during 1992–1997, estimated from ocean observations and a general circulation model. *Journal of Geophysical Research* 107(C9), 3118, <https://doi.org/10.1029/2001JC000888>.
- St. Laurent, L., T. Ijichi, S.T. Merrifield, J. Shapiro, and H.L. Simmons. 2019. Turbulence and vorticity in the wake of Palau. *Oceanography* 32(4):102–109, <https://doi.org/10.5670/oceanog.2019.416>.
- Tozuka, T., and T. Yamagata. 2003. Annual ENSO. *Journal of Physical Oceanography* 33:1,564–1,578, <https://doi.org/10.1175/2414.1>.
- Vecchi, G.A., and D.E. Harrison. 2000. Tropical Pacific sea surface temperature anomalies, El Niño, and equatorial westerly wind events. *Journal of Climate* 13:1,814–1,830, [https://doi.org/10.1175/1520-0442\(2000\)013<1814:TPSSSTA>2.0.CO;2](https://doi.org/10.1175/1520-0442(2000)013<1814:TPSSSTA>2.0.CO;2).
- Wang, C., and J. Picaut. 2004. Understanding ENSO physics: A review. Pp. 21–48 in *Earth's Climate: The Ocean-Atmosphere Interaction*. Geophysical Monograph Series, 147, C. Wang, S.-P. Xie, and J.A. Carton, eds, American Geophysical Union, Washington, DC.
- Wolanski, E., P.L. Colin, J. Naithani, E. Deleersnijder, and Y. Golbuu. 2004. Large amplitude, leaky, island-generated, internal waves around Palau, Micronesia. *Estuarine, Coastal and Shelf Science* 60:705–716, <https://doi.org/10.1016/j.ecss.2004.03.009>.
- Wyrki, K. 1975. El Niño—The dynamic response of the equatorial Pacific Ocean to atmospheric forcing. *Journal of Physical Oceanography* 5:572–584, [https://doi.org/10.1175/1520-0485\(1975\)005<0572:ENTDRO>2.0.CO;2](https://doi.org/10.1175/1520-0485(1975)005<0572:ENTDRO>2.0.CO;2).
- Zeiden, K.L., D.L. Rudnick, and J.A. MacKinnon. 2019. Glider observations of a meso-scale oceanic island wake. *Journal of Physical Oceanography* 49(9):2,217–2,235, <https://doi.org/10.1175/JPO-D-18-0233.1>.

## ACKNOWLEDGMENTS

This study was supported by the ONR project Flow Encountering Abrupt Topography (FLEAT): N00014-15-1-2488 (MCS and DLR), N00014-16-WX01186 (HWW, DWW, WJT, ZRH), N00014-15-12285 (BDC, GP) and the National Oceanographic Partnership Program (NOPP): N00014-15-12598 (BDC, GP). Temperature logger deployments were first supported by internal funds of the Coral Reef Research Foundation (CRRF) and later by the FLEAT initiative.

We thank the Instrument Development Group at Scripps Institution of Oceanography for all operations of the Spray gliders, and the staff of CRRF in Palau for their support of glider operations, particularly Lori J.B. Colin, Matt Mesubed, and Emilio Basilius. CRRF and staff are also thanked for logistical support for R/V *Roger Revelle* cruises in Palau. Special thanks are extended to the captain and crew of R/V *Revelle* during deployment, recovery, and survey legs of this project, and to Andrew Quaid and Ian Martens for their extraordinary efforts in preparation, deployment, and recovery of the moorings, and for their technical support during the ship surveys. Joel Wesson provided outstanding support during the cruise. This study was conducted using EU Copernicus Marine Service Information and data available from the European Center for Medium-Range Weather Forecasting.

We thank the Palau National Government for permission to carry out the research in Palau. The state governments of Angaur, Hatohobei, Kayangel, and Koror are also thanked for allowing access to their coastal waters for water temperature monitoring.

## AUTHORS

**Martha C. Schönau** ([martha.schonau@appliedoceansciences.com](mailto:martha.schonau@appliedoceansciences.com)) is Senior Scientist, Applied Ocean Sciences, Fairfax Station, VA, USA. **Hemantha W. Wijesekera** is Oceanographer, Naval Research Laboratory, Stennis Space Center, MS, USA. **William J. Teague** is Research Scientist, NVision Solutions Inc., Diamondhead, MS, USA. **Patrick L. Colin** is Director, Coral Reef Research Foundation, Koror, Palau. **Ganesh Gopalakrishnan** is Project Scientist, **Daniel L. Rudnick** is Professor, and **Bruce D. Cornuelle** is Research Oceanographer, all at Scripps Institution of Oceanography, University of California San Diego, La Jolla, CA, USA. **Zachariah R. Hallock** is Research Scientist, NVision Solutions Inc., Diamondhead, MS, USA. **David W. Wang** is Oceanographer, Naval Research Laboratory, Stennis Space Center, MS, USA.

## ARTICLE CITATION

Schönau, M.C., H.W. Wijesekera, W.J. Teague, P.L. Colin, G. Gopalakrishnan, D.L. Rudnick, B.D. Cornuelle, Z.R. Hallock, and D.W. Wang. 2019. The end of an El Niño: A view from Palau. *Oceanography* 32(4):32–45, <https://doi.org/10.5670/oceanog.2019.409>.

## COPYRIGHT & USAGE

This is an open access article made available under the terms of the Creative Commons Attribution 4.0 International License (<https://creativecommons.org/licenses/by/4.0/>), which permits use, sharing, adaptation, distribution, and reproduction in any medium or format as long as users cite the materials appropriately, provide a link to the Creative Commons license, and indicate the changes that were made to the original content.